Homework 3 solution from group 3

1 1D FDTD

1.1 Implementation

The electric field is determined using the values of the magnetic field from the previous iteration. However, only the interior 2:Nx-1 of the electric field is updated. The derivative of the magnetic field is obtained by subtracting the magnetic field value of index 1:Nx-2 from the magnetic field value of index 2:Nx-1. Since the spatial dimension of the magnetic field has a length of Nx-1, a vector with Nx-2 elements is generated. eps_rel has the same grid as the electric field and is indexed in the same way. Subtracting the source currents gives the new electric field. In this process, the source time is calculated according to the change in time between the current and the electric field. A complex exponential function is used to oscillate the carrier. This creates a complex source amplitude and results in the entire FDTD implementation using a complex field. In this process, all spatial coordinates of the magnetic field are updated. and there are no boundary values to be preserved. At the end of the 1D FDTD implementation, the electric and magnetic fields are converted to a common coordinate system by interpolating the magnetic field from fractional to integer exponents.

1.2 Simulation in homogeneous medium

Simulate the propagation of an ultrashort pulse in a dispersion-free dielectric medium ϵ(x)=1.

Apparently, after colliding on the wall, field can bounce back and continue propagating because perfect conducting boundary condition is used in this task. We set the value of boundaries directly as zeros. Two boundaries act as the behavior of metal; therefore, reflection can be observed in this simulation.

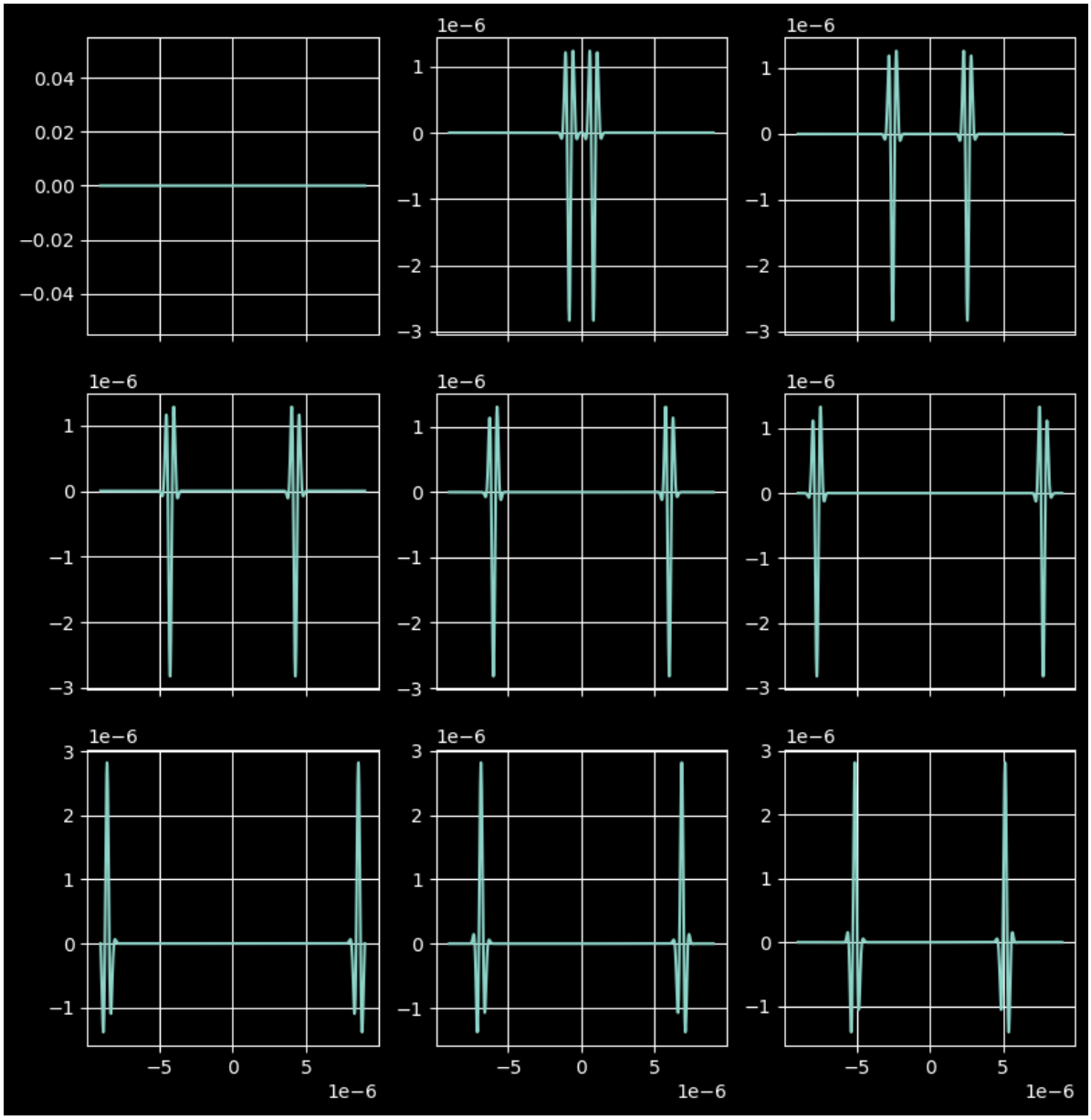

Figure 1: 1d FDFT in homogeneous medium

1.3 Simulation in inhomogeneous medium

See what happens when the pulse hits the interface between two different dielectric media with permittivities $\epsilon\ 1 = 1$ and $\epsilon\ 2 = 4$, the interface should be located at a distance of 4.5 µm in positive direction from the center of the computational domain.

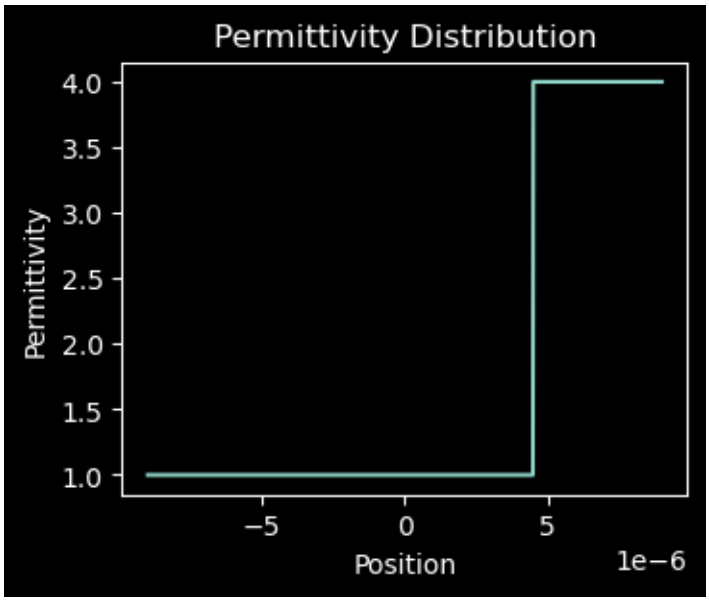

Figure 2: The inhomogeneous permittivity distribution

The propagation behavior is shown below, blue line represents the amplitude of poynting vecotor, red line represents permittivity distribution.

In this case, after the field across through the interface of different material, both transmission and reflection can be observed. Based on the formula $\frac{(n1-n2)^2}{(n1+n2)^2}$, the reflectance can be derived as 11%. This can be also confirmed in the simulation that most part of field can transmit through the interface. Similarly, as previous task, after fields collide on the metal boundary, they can be totally reflected and keep propagating.

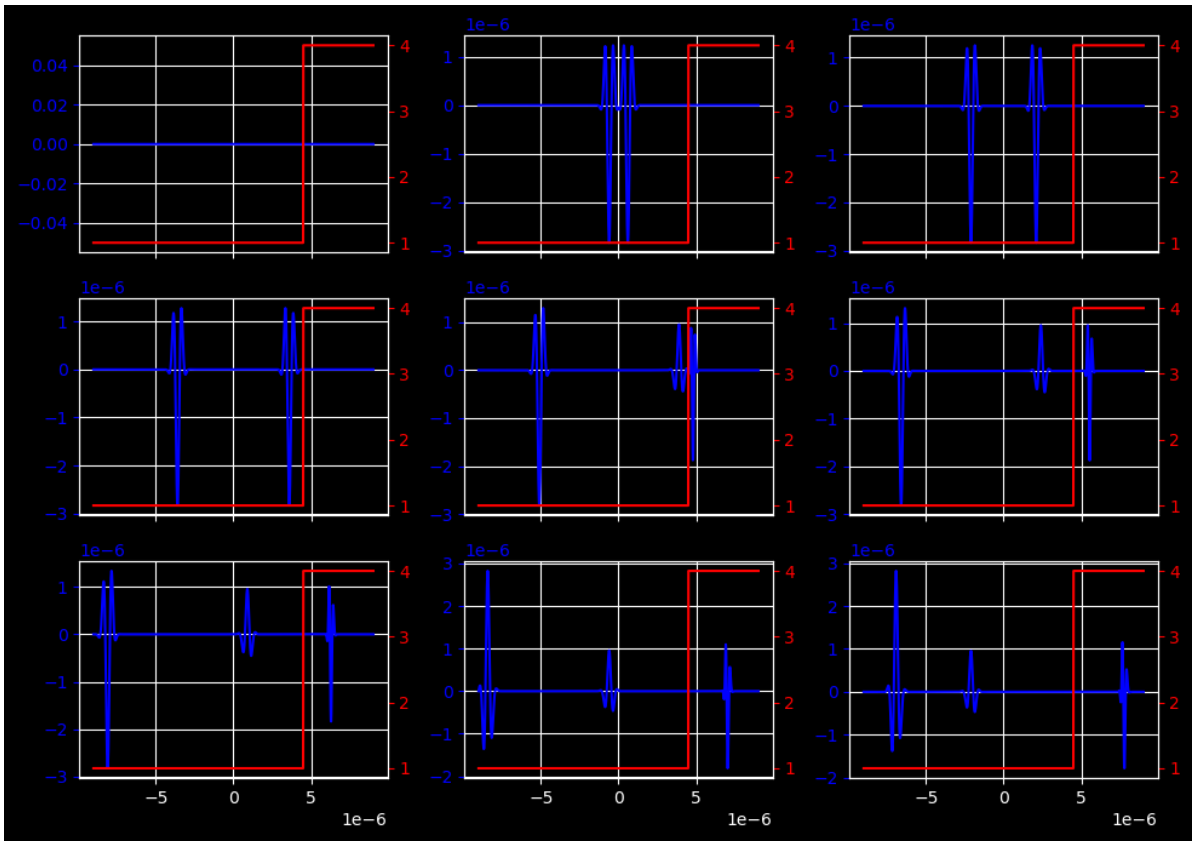

Figure 3: 1d FDFT in inhomogeneous medium

2 3D FDTD

2.1 implementation

The electric field components can be calculated with equations

$$E_x|^{n+1}_{i+1/2,j,k} = E_x|^{n}_{i+1/2,j,k} + \frac{\Delta t}{\epsilon_0 \epsilon_{i+1/2,j,k}} \left[\frac{H_z|^{n+1/2}_{i+1/2,j+1/2,k} - H_z|^{n+1/2}_{i+1/2,j-1/2,k}}{\Delta y} - \frac{H_y|^{n+1/2}_{i+1/2,j,k+1/2} - H_y|^{n+1/2}_{i+1/2,j,k-1/2}}{\Delta z} - j_x|^{n+1/2}_{i+1/2,j,k} \right] \tag{1}$$

$$E_y|^{n+1}_{i,j+1/2,k} = E_y|^{n}_{i,j+1/2,k} + \frac{\Delta t}{\epsilon_0 \epsilon_{i,j+1/2,k}} \left[\frac{H_x|^{n+1/2}_{i,j+1/2,k+1/2} - H_x|^{n+1/2}_{i,j+1/2,k-1/2}}{\Delta z} - \frac{H_z|^{n+1/2}_{i+1/2,j+1/2,k} - H_z|^{n+1/2}_{i-1/2,j+1/2,k}}{\Delta x} - j_y|^{n+1/2}_{i,j+1/2,k} \right] \tag{2}$$

$$E_z|^{n+1}_{i,j,k+1/2} = E_z|^{n}_{i,j,k+1/2} + \frac{\Delta t}{\epsilon_0 \epsilon_{i,j,k+1/2}} \left[\frac{H_y|^{n+1/2}_{i+1/2,j,k+1/2} - H_y|^{n+1/2}_{i-1/2,j,k+1/2}}{\Delta x} - \frac{H_x|^{n+1/2}_{i,j+1/2,k+1/2} - H_x|^{n+1/2}_{,j-1/2,k+1/2}}{\Delta y} - j_z|^{n+1/2}_{i,j,k+1/2} \right] \tag{3}$$

and the magnetic field components can be calculated as

$$H_x|^{n+3/2}_{i,j+1/2,k+1/2} = H_x|^{n+1/2}_{i,j+1/2,k+1/2} + \frac{\Delta t}{\mu_0} \left[\frac{E_y|^{n+1}_{i,j+1/2,k+1} - E_y|^{n+1}_{i,j+1/2,k}}{\Delta z} - \frac{E_z|^{n+1}_{i,j+1,k+1/2} - E_z|^{n+1}_{i,j,k+1/2}}{\Delta y} \right] \tag{4}$$

$$H_y|^{n+3/2}_{i+1/2,j,k+1/2} = H_y|^{n+1/2}_{i+1/2,j,k+1/2} + \frac{\Delta t}{\mu_0} \left[\frac{E_z|^{n+1}_{i+1,j,k+1/2} - E_z|^{n+1}_{i,j,k+1/2}}{\Delta x} - \frac{E_x|^{n+1}_{i+1/2,j,k+1} - E_x|^{n+1}_{i+1/2,j,k}}{\Delta z} \right] \tag{5}$$

$$H_z|^{n+3/2}_{i+1/2,j+1/2,k} = H_z|^{n+1/2}_{i+1/2,j+1/2,k} + \frac{\Delta t}{\mu_0} \left[\frac{E_x|^{n+1}_{i+1/2,j+1,k} - E_x|^{n+1}_{i+1/2,j,k}}{\Delta y} - \frac{E_y|^{n+1}_{i+1,j+1/2,k} - E_y|^{n+1}_{i,j+1/2,k}}{\Delta x} \right] \tag{6}$$

We assume the range of x, y, z-axis are [0, Nx], [0, Ny], [0, Nz]. The i index of E_x component shifts a half spacial step, and the range of it becomes [0.5, Nx+0.5]. The last position is not in the range of [0, Nx] and should not be counted in the computation. Therefore, the size of E_x is (Nx-1, Ny, Nz) instead (NX, Ny, Nz).Likewise, the size of E_y and E_z are (Nx, Ny-1, Nz) and (Nx, Ny, Nz-1), and the size of H_x, H_y, H_z are (Nx, Ny-1, Nz-1), (Nx-1, Ny, Nz-1), and (Nx-1, Ny-1, Nz), respectively.

In PEC boundary conditions, the tangential E-fields at the boundaries are not updated and keep in 0. Therefore, only the grid points in range of [0:Nx-1, 1:Ny-1, 1:Nz-1] in E_x field, [1:Nx-1, 0:Ny-1, 1:Nz-1] in E_y field and [1:Nx-1, 1:Ny-1, 0:Nz-1] in E_z field need to be updated. On the contrary, the tangential H-fields have to be updated and the normal H-field keep in 0 at the boundaries. The grid points in range of [1:Nx-1, 0:Ny-1, 0:Nz-1] in H_x field, [0:Nx-1, 1:Ny-1, 0:Nz-1] in H_y field, and [0:Nx-1, 0:Ny-1, 1:Nz-1] in H_z field need to be updated. These points are called inner grid points.

The derivatives of the magnetic field components are calculated at the inner grid points without boundary values. The source term is subtracted from the derivatives of the magnetic field and then multiplied by the interpolated inverse derivative, which creates a new electric field. The old electric field values from the inner grid points are added to the new field. If so, the field is interpolated into the grid of eps_rel before the z-sheet is extracted at the z-index specified by z_ind. To implement the interpolation, we apply `np.pad` function to pad the edge values in the front and back of the electric field array in corresponding axis (x in E_x field, y in E_y field, and z in E_z field), and calculate the average of the 2 padded array. After the electric field components have been taken into account, the new magnetic field components are calculated. The magnetic field components are stored in a temporary array and the same interpolation method is used to calculate the average of the old and the new magnetic field. In this way, the magnetic field can be determined in the same time step and the same space position as the stored electric field components.

We consider the edge values as the missing values in the interpolation. For example, $E_x(0, :, :)$ is equal to $E_x(1, :, :)$ in our implementation. In this case, the values of the points at the boundaries do not change in the interpolation step.

2.2 Simulation in homogeneous medium

When simulating the propagation of electromagnetic fields in a homogeneous medium with a refractive index $n = 1$, the 3D FDTD method is used. Five grid points were defined along the z-direction. and the grid resolution was set to $\Delta r = 30nm$. A z-polarised line current with a Gaussian spatial profile along x and y at the centre of the computational domain was used for excitation. The duration of the simulation is $T = 10$ fs. and the z-polarised current source excites only the z-component of the electric field. Since the current density is constant along the z-axis and the z-component of the electric field is not affected by the PEC boundary in

the z-direction, there are no x- and y-components of the electric field and no z-component of the magnetic field.

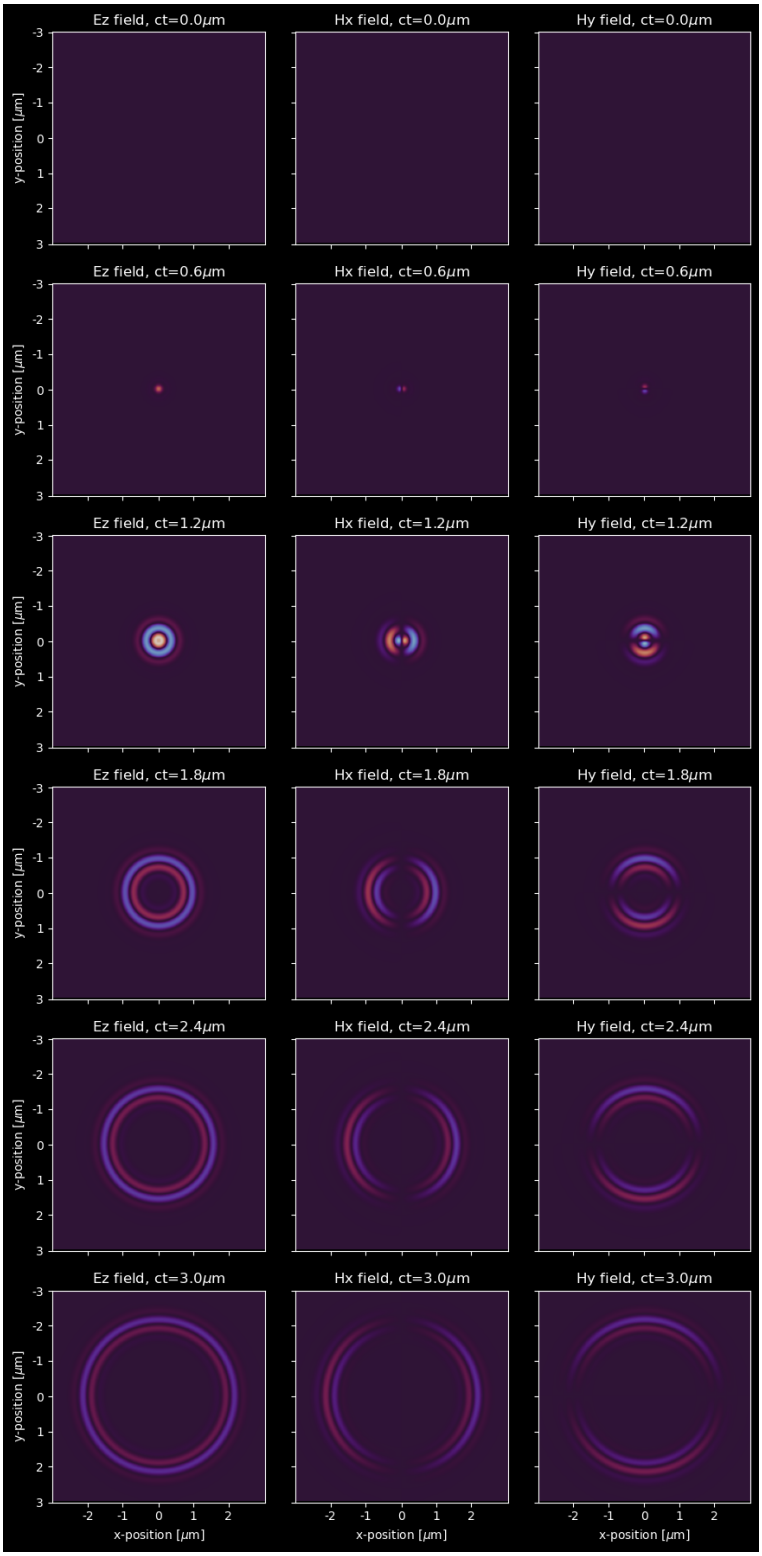

Figure 4: Ez, Hx, and Hy field created by 3d FDTD in homogeneous medium. Spacial and temporal resolutions are set to Δr=30nm and Δt = Δx/2c = 5e-17s

2.2.1 PEC boundaries

Starting from step (a), the upper arrow indicates a positive charge placed on the left-hand side, while a negative charge is placed on the right-hand side. Since it is a perfectly electric conductor, the negative charge in the lower part of the figure will be attracted to the positive charge in the upper part, causing it to appear on the left-hand side. Conversely, the positive charge in the lower part will be attracted to the negative charge in the upper part, causing it to appear on the right-hand side. As a result, the lower electric field can exhibit an opposite direction to the upper electric field. Similarly, step (b) can be also understood in this way.

Regarding step (c), based on right hand rule, electric field rotates counterclockwise and points in the page at the boundary. Consequently, due to the characteristic of perfectly electric conductor, the induced electric field points out of the page at the boundary and rotates also counterclockwise, causing the induced magnetic field pointing in the same direction as upper one. Similarly, step (d) can be explained in this manner.

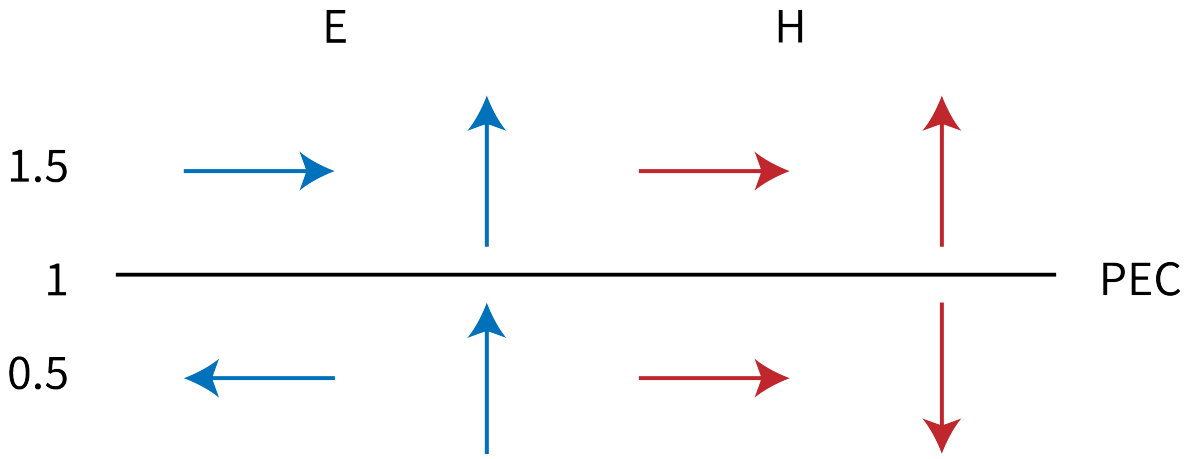

Figure 5: PEC boundary condition

3 Convergence test

3.1 1D case

3.1.1 dx convergence test

The error is calculated as follows:

$$e = \left| \frac{E_{tot} - E^*_{tot}}{E^*_{tot}} \right|$$

but since E^*_{tot} is unknown, we approximate it with the result with the smallest step size. Besides, because the number of grid points is not constant in this experiment, the relative error cannot be calculated with the square root of sum of the squared magnitude. Instead, it is approximated by the value of peak power of field for the end of time evolution.

This simulation is implemented under explicit scheme. The explicit scheme exhibits an growth due to the instability that causes an amplification of high frequencynoise. Therefore, the relative error would just diverge in this range of simulation step size.

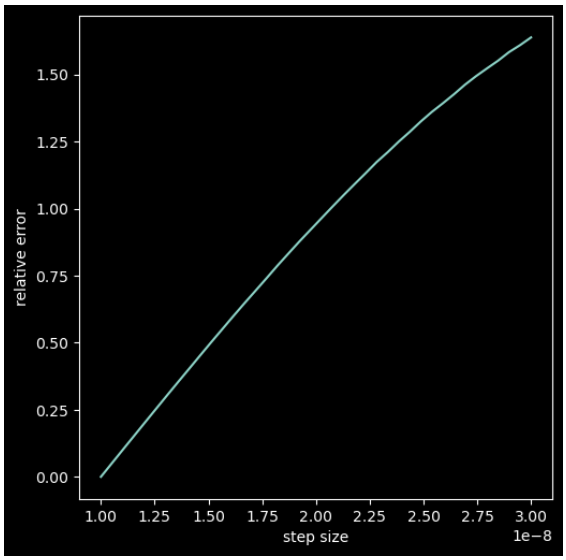

Figure 6: Convergence of the 1d FDTD in dependence of the lateral step size Δx.

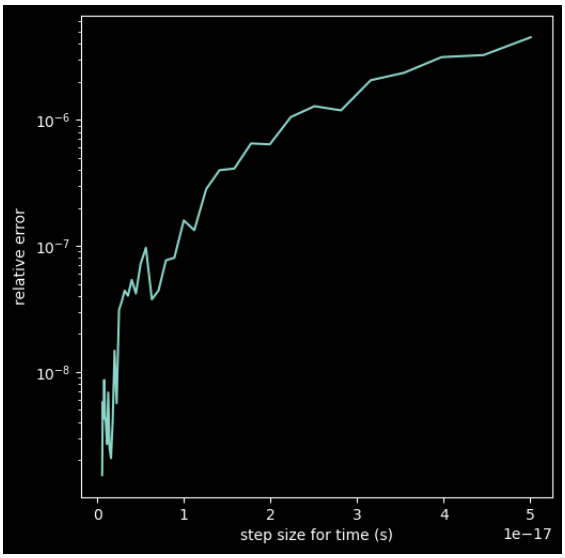

Figure 7: Convergence of the 1d FDTD in dependence of the temporal resolution Δt.

3.1.2 dt convergence test

In this experiment, dx is fixed, and dt acts as variable in the function. In order to be valid for the correlation between dx and dt, dx is taken as 30 nanometer when dt ranges from 15

to 30 nanometer over 2 times speed of light. In this case, square root of sum of the squared magnitude of the difference between the propagated field is applied because the grid points are constant for different time steps.

This is in explicite scheme; therefore, for both temporal and spatial test, the relative error just increases with respect to the larger step size.

3.2 3D case

In this section, we will discuss the influence of the discretization onto the accuracy of the obtained solution. First, we will have a look at the influence of Δt. The relative error e is given by the root mean square error (RMSE) between the propagated electric field Ez and the true result Ez^* at the time t = 60fs:

$$e = \sqrt{\frac{\sum_{i=1,j=1}^{Nx,Ny} E_z^*(i,j) - E_z(i,j)}{NxNy}}$$

The true result was approximated by the result at the smallest Δt(1e-18s), and Δt values are in the range of (5e-18, 5e-17)s. Δx was set to 30nm. Figure 8 shows the convergence of the 3d FDTD method with respect to Δt. As expected, the relative error increases alone the increasing of Δt. The relative errors are relative small for all tested Δt.

The influence of the spacial resolution is tested. Because the shapes of output fields are different, we extract the grid points in specific positions to make sure the number of grid points keep in constant before calculating the RMSE. Δt is set to 2.5e-18s. For reducing the computation time, the spacial span is set to $x = y = 1.5\mu m$, time span to t=4.5fs, and output step to 40. The result is shown in Fig. 9. The influence of the spacial resolution have a similar behaviour as the temporal resolution. It increases with respect to the larger step size and keeps in a relative small values.

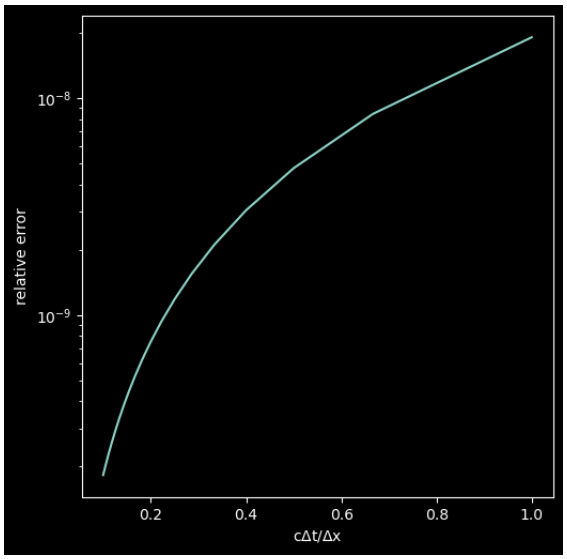

Figure 8: Convergence of the 3d FDTD in dependence of the temporal resolution Δt.

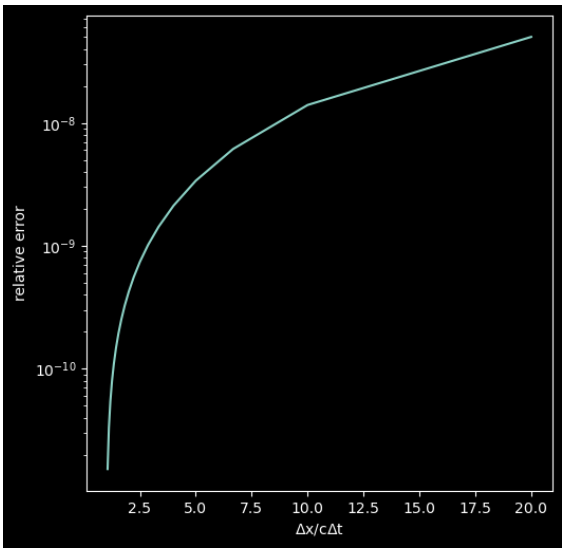

Figure 9: Convergence of the 3d FDTD in dependence of the spacial resolution Δx.